Heliyon 8 (2022) e10689

Contents lists available at ScienceDirect

Heliyon

journal homepage: www.cell.com/heliyon

Research article

Inexpensive and easily replicable precipitation of CuO nanoparticles for low temperature carbon monoxide and toluene catalytic oxidation

Hippolyte Todou Assaouka [a], Daniel Manhouli Daawe [b], Roussin Lontio Fomekong [c], Issah Njiawouo Nsangou [a], Patrick Mountapmbeme Kouotou [b,d,*]

[a] Department of Chemistry, Faculty of Sciences, University of Maroua, P.O. Box.: 55, Maroua, Cameroon
[b] National Advanced School of Engineering, University of Maroua, P.O. Box. 46, Maroua, Cameroon
[c] Higher Teacher Training College, University of Yaounde 1, P.O. Box 47, Yaoundé, Cameroon
[d] Institute of Engineering Thermophysics, Chinese Academy of Sciences, Beijing 100190, China

ARTICLE INFO

Keywords:
Catalytic oxidation
Copper oxide
Precipitation
Carbon monoxide
Toluene

ABSTRACT

Herein CuO nanoparticles (NPs) with nanostructures were prepared by precipitation method using hydrate copper sulfate ($CuSO_4.5H_2O$) and sodium hydroxide followed by heat treatment at 400 °C. The as-prepared CuO NPs with nanostructures were investigated using X-ray diffraction (XRD), Fourier Transformed Infra-red spectroscopy (FTIR), Raman spectroscopy, Scanning electron microscopy (SEM), X-ray photochemical spectroscopy (XPS), Energy dispersive spectroscopy (EDS), and Ultra-violet-visible (UV-vis) spectroscopy. In order to evaluate the reducibility, temperature programmed reduction (H_2-TPR) was applied. More importantly, CuO NPs was successfully tested as catalyst towards the total conversion of carbon monoxide (CO) and toluene (C_7H_8). Both XRD and Raman analysis as well as FTIR show that the sample exhibited a monoclinic spinel structure. SEM images indicate that CuO NPs are well-covered by grains size exhibiting homogeneous morphology composed of very fine interconnected particles with an apparent porosity. The sample was made up of Cu and O, according to the XPS and EDS measurements. The band gap energy obtained from optical property analysis is ~2.65 eV. The catalytic performances of CuO NPs can be assigned to the combined effects of crystal structure, morphology, surface oxygen mobility, redox property and the higher specific surface area (~87 m^2/g). More precisely XPS and H_2-TPR data suggests that, the conversion of CO and C_7H_8 over CuO NPs follows a Mars-van Krevelen type mechanism. More importantly CuO NPs catalysts is reusable and exhibited good stability in the prolonged isothermal test. Thus, CuO NPs is confirmed as an efficient and inexpensive catalysts for CO and C_7H_8 conversion at low temperatures.

1. Introduction

The increasing environmental regulations and people awareness of the need for environmental protection as well as the urgent need of the decontamination of polluted atmosphere have drawn the attention of many researchers [1]. Carbone monoxide (CO) and toluene (C_7H_8) generally emitted from several sources including mobile sources (automobiles), stationary sources (industrial facilities) and area sources (e.g., agricultural areas and towns) are responsible of the atmospheric pollution that seriously impact the environment and human health. In fact, C_7H_8 causes the formation of smog, acid rain and also contributes to the ozone layer depletion. Meanwhile, CO is harmful when breathed since it can easily displace oxygen in the human blood and deprives vital organs of oxygen including the heart and the brain. Moreover, most industrial processes like methanol manufacturing and gas shift process involves the oxidation of CO [2, 3].

Catalytic oxidation process is one of the most interesting elimination techniques of Volatile Organic Compounds (VOCs) regarding its efficiency and the cost of implementation [4]. The most used catalysts are made of precious metals such as Au, Pd and Ag [5, 6]. However they are scare, exhibits low thermal stability, poisoning tendency and low selectivity in some oxidation reactions [7]. Transition metal oxides (TMOs) appears as alternative regarding their availability, excellent thermal stability and flexibility [5]. Today, TMOs catalysts with competitive reactivity are currently being improved and those made of copper have presented special advantages [7, 8, 9, 10, 11, 12, 13]. In fact, copper

* Corresponding author.
E-mail address: mkpatrick1982@gmail.com (P.M. Kouotou).

https://doi.org/10.1016/j.heliyon.2022.e10689
Received 3 June 2022; Received in revised form 17 July 2022; Accepted 14 September 2022

oxide (CuO) nanoparticles (NPs) are among of catalysts that have caught attention of materials chemistry researchers over the past two decades, because of their abundance, non-plasmoni, low-cost materials and their multiple uses in heterogeneous catalysis [14, 15, 16, 17]. Moreover CuO NPs generally exhibits remarkable performance towards VOCs catalytic oxidation, and especially in the low temperature CO oxidation [18, 19]. The physico-chemical properties control of the catalysts from the synthesis process can enable the improvement of the catalytic performance of the latter mentioned [20].

Numerous techniques including co-precipitation, sol-gel [14], solvothermal [15], thermal decomposition [16], flame synthesis [17], and chemical vapor deposition [18], were applied for the preparation of CuO nanoparticles. The as-synthesized material was applied in different fields including electrode materials, gas sensors and adsorbents as well as an efficient catalysts for several heterogeneous catalytic processes [14, 15, 16, 17, 18]. Compared with the synthesis approaches outlined above, co-precipitation has caught considerable attention because of its relatively ease and low-cost processing. In fact, the synthesis is generally achieved at relatively low-temperature and ambient pressure [21, 22]. This synthesis method and the processing parameters have been reported to generally influence the microstructure, particle size and redox properties of the as-prepared CuO catalyst and which might in consequence improve their physico-chemical properties, thus their catalytic activity [23]. Thus, a great attention and serious efforts to control the preparation of nano-structured CuO materials with tuned grains size and morphology have been made and the principal factors responsible of the remarkable catalytic performance were studied [24]. Accordingly, the physico-chemical and redox properties which are crucial and of capital importance in the improvement of the catalytic performance should be tuned although it is challenging.

In the present investigation, CuO NPs catalysts was prepared by precipitation route. X-ray diffraction (XRD), Raman spectroscopy, Fourier Transformed Infrared spectroscopy (FTIR), Scanning electron microscopy (SEM), Energy dispersive spectroscopy (EDS), and X-ray photochemical spectroscopy (XPS) have all been used to analyze the as-prepared catalyst. Moreover, temperature-programmed reduction (H_2-TPR) was used to assess reduction property of CuO NPs, while UV-visible spectroscopy was used to quantify the optical energy band gap (E_g^{opt}). More importantly, the catalytic activity towards the total conversion of CO and C_7H_8 was evaluated. The performance of the obtained catalyst has been assigned to their tailored physico-chemical properties.

The aim of this work is (1) to prepare, systematically characterized and study the catalytic activity of CuO NPs catalyst for CO and C_7H_8; (2) to investigate the stability and durability of CuO NPs catalyst obtained by simple and reproducible precipitation route in the catalytic oxidation process. Moreover, in-situ DRIFTS technology was used to explore the possible reaction mechanism of CO and toluene oxidation on the surface of CuO catalysts.

2. Experimental

2.1. Catalyst preparation technique

The precipitation method was used to synthesized pure CuO NPs, from hydrate copper sulfate ($CuSO_4.5H_2O$). 4.99 g of hydrated copper sulfate have been dissolved in 100 mL of 95% ethanol. NaOH solution (2M) was added gradually with stirring (2 h) until the pH reached 13.5. The obtained precipitate was rinsed with deionized water five times before being dried in an oven at 105 °C for 24 h. Finally, the resulted product was calcined at 400 °C for 4 h in an electric furnace.

2.2. Systematic characterization

The crystal structure of CuO NPs was studied by XRD at room temperature with powder diffraction equipment using Cu Kα (λ = 0.154056 nm) radiation from Bruker (D8 Focus at 40 kV and 150 mA). CuO sample was scanned within 2 θ, ranging from 20 to 80°, with a scan rate of 0.025° step per second. The obtained sample was identified using the Joint Committee on Powder Diffraction Standards (JCPDS) database. The diameter of CuO NPs grains size was determined from the prominent peak using Scherrer equation (Eq.1):

$$D = \frac{k\lambda}{\beta cos\theta} \quad (1)$$

In which D is the average crystallite particle size, k represents the shape factor (0.9), λ is the wavelength, β is the line broadening, and θ is the diffraction angle. The surface specific area was performed using a nitrogen physisorption equipment (NOVA3000, Quanta-chrome, China) and calculated by Brunauer–Emmett–Teller (BET) equation. Before the investigation, CuO NPs were exposed at 300 °C under vacuum for 3 h to remove any impurities, then adsorbed with nitrogen at ~196 °C and followed by a desorption at room temperature. H_2-TPR was investigated on a chemical adsorption apparatus (PCA-1200, Beijing Builder) associated with a quartz reactor and TCD detector. Prior to the catalytic test, 60 mg samples were pretreated for 40 min in Argon (Ar) flow from room temperature to 500 °C and then cooled down to 100 °C. The H_2-TPR analysis was carried out on samples that were exposed to 5% H_2 dilute in Ar atmosphere at a flow rate of 30 mL min^{-1} using heating rate of 10 °C min^{-1} until the temperature reached 900 °C. The possible functional groups present on CuO NPs surface were determined by the mean of Fourier Transform Infrared (FTIR) spectrometer (Perkin-Elmer), operating within the wavenumber ranging from 4000 cm^{-1} to 400 cm^{-1}, with a ramp of 3 °C min^{-1} and a flow rate of 5% H_2/O_2 diluted in Ar (0.05 L min^{-1}). Raman spectrum was collected using a DXR 2 Raman spectroscope (Thermo Fisher Scientific, Madison, WI, USA) equipped with LASER source (780 nm) for the excitation. The morphology of the nanoparticles was studied at room temperature using in sit ultra-high-resolution SEM (S-4800 Hitachi, USA). The KRATOS AXIS Ultra XPS instrument was used to perform the XPS analysis. The UV-visible absorption spectrum was recorded in the range of 300–900 nm by an Ultra Violet -visible spectrophotometer (UV-2550, SHIMADZU, China). The optical energy band gap (Eg) was determine applying Tauc's equation (Eq.2):

$$Ahv = A\left(hv - E_g\right)^n \quad (2)$$

Where α represents the absorption coefficient, A is assigned to refractive index, hν represents the photon.

2.3. Catalytic performance test

The catalytic activity of CuO NPs toward the complete oxidation of CO and C_7H_8 was examined. The tests were carried out in a tubular (inside Ø, 6 mm) fixed-bed reactor system. During the catalytic testing, 60 mg of catalyst were introduced within a fixed-bed reactor, and the reaction temperature was monitored using a thermocouple (k-type) disposed in contact with the catalyst bed. The inlet gas was composed of 5% CO and 20% O_2 diluted in Ar and at a total flow rate of 60 mL min^1, which correspond to a gas hourly space velocity (GHSV) of 72 000 mL^3 g^{-1} h^{-1}. As for C_7H_8, the reaction gas mixture was composed of 500 ppm C_7H_8 and 20% O_2/Ar, in a total gas flow of 75 mL min^{-1}, (GHSV: 20 000 $mLg^{-1}h^{-1}$). Gaseous C_7H_8 was generated via an Ar bubbler from a bottle of C_7H_8 (liquid) cooled in a 0 °C isothermal bath (ice-water). To avoid C_7H_8 condensation on the reactor walls, a heating band was employed to heat up to 100 °C the entire reaction gas lines. The flow rate was adjusted using digital mass flow controllers. The evaluation of the catalytic performances of the as-synthesized material was carried out at a constant pressure of 1 atm, within the temperature range of 50–450 °C. A flame ionization detector (FID) in a gas chromatograph (GC-6890A) equipped with a thermal conductivity detector (TCD) was used to detect reactants molecules and products at a specific temperature. The experimental setup for the catalytic test of C_7H_8 is shown in Figure 1. All data points were

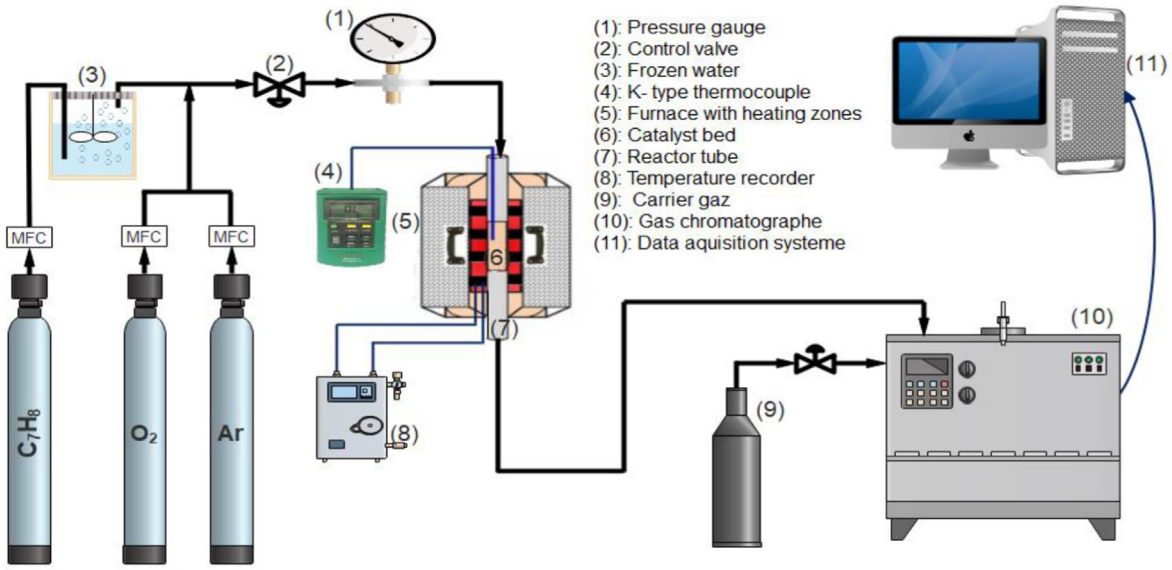

Figure 1. Experimental setup for the catalytic test of C_7H_8.

acquired by averaging 2 test results. The oxidation percentage of CO and C_7H_8 was determined using the following relationships (Eq.3), respectively:

$$\begin{aligned} \text{CO}\ (\%) &= \left[(\text{CO})_{\text{inlet}} - (\text{CO})_{\text{outlet}}\right] \times 100 \text{ and } C_7H_8(\%) \\ &= \left[(C_7H_8)_{\text{inlet}} - (C_7H_8)_{\text{outlet}}\right] \times 100 \end{aligned} \quad (3)$$

3. Results and discussion

3.1. The crystal structure

In order to evaluate the crystal structure of the as-synthesized CuO NPs, XRD was performed and shown in Figure 2. Figure 2a displays the powder XRD diffraction spectrum of CuO NPs exhibiting two prominent peaks located at 35.3 (−111) and 38.6 (111) [25]. The observed major reflections can be assigned to the planes of the monoclinic structure as correlated with the JCPDS (file No.:48-1548) and that reported in the literature [26, 27]. The higher crystallinity is evidenced by the strong diffraction peaks of CuO. In addition, no impurities phase was found. The average particles size of the CuO NPs was estimated at ~14 nm.

The Fourier Transform Infra-Red spectrum displaying the characteristic peaks of CuO NPs within wavenumber range of~432 cm^{-1} to ~3252 cm^{-1} is presented in Figure 2b. The peaks located at ~661, ~601, ~496, and ~432 cm^{-1} are ascribed to the vibrational modes of Cu–O chemical bond characteristic of CuO NPs with monoclinic structure [25]. The peak at ~1573 cm^{-1} might be due to the bending mode of H_2O molecules, whereas the most intense one (~3252 cm^{-1}) correspond to the stretching vibration mode of OH from molecular H_2O. These results is in close agreement with earlier reported CuO NPs in the literature [28].

To further analyze the crystalline structure of the CuO NPs catalyst, Raman analysis was performed and the corresponding spectrum is depicted in Figure 3. It is well established that CuO NPs exhibits three distinct modes at ambient conditions: ~296 cm^{-1} (A1g), ~346 cm^{-1} (B1g) and ~636 cm^{-1} (B2g) [29]. In the present work as displayed in Figure 3, the peaks at ~294 cm^{-1} (A1g), ~342 cm^{-1}(B1g), and ~632 cm^{-1}(B2g) are attributed to the vibration modes of Cu–O bond of CuO NPs catalyst. The obtained frequencies here are slightly shifted toward lower values and the bands broaden due to effects of quantum confinement generally observed for samples with relatively smaller crystallite sizes [30]. It's worth noting that the A1g peak exhibit higher intensity than that of B1g and B2g bands, indicating high degree of CuO crystallization as revealed by the XRD analysis, in perfect agreement with the literature [16]. The large band at ~1119 cm^{-1} can be assigned to multi-phonon [31, 32]. The peak at ~722 cm^{-1} has been reported to be an indication of the occurrence of oxygen vacancies in the CuO NPs lattice [33].

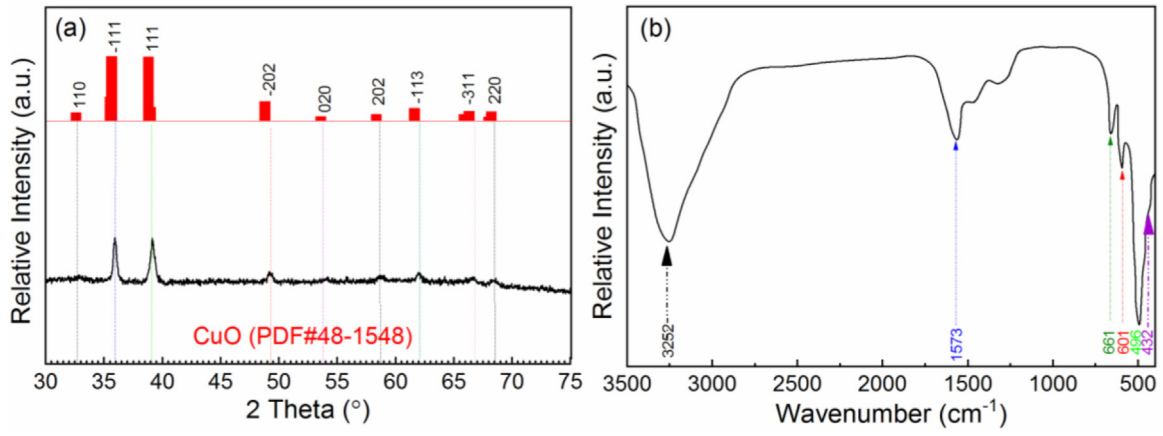

Figure 2. (a) X-ray diffraction and (b) Fourier Transformed Infra-red spectra of CuO NPs.

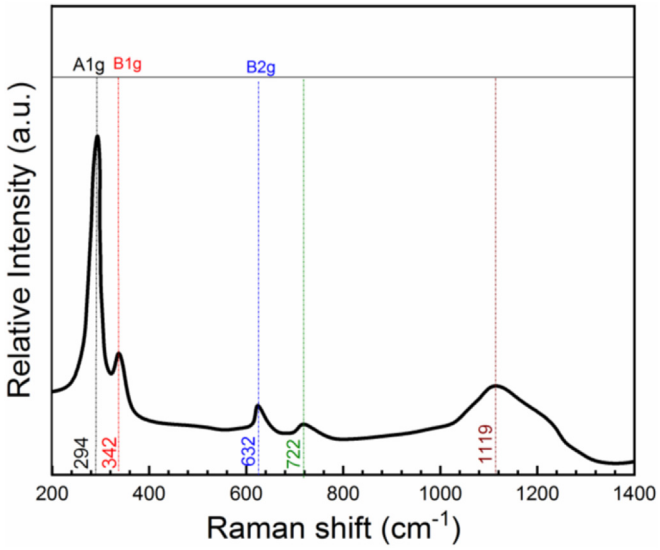

Figure 3. Raman spectrum of CuO NPs prepared by precipitation.

3.2. Morphological microstructure

SEM analysis was used to investigate the morphology of CuO NPs and display in Figure 4. Figure 4 (a and b) shows low and higher-magnification micrographs of CuO NPs. The sample shows homogeneous surface, well-covered with fine interconnected particles with an apparent porosity. From the higher magnification SEM images, it is obvious that, CuO samples are composed of small particles resulting of the agglomeration of smallest micro-crystal. Such a surface morphology and narrow particles size with porous-like structure which are responsible of the large specific surface area (~87 m^2/g) generally offer more exposed surface contact for reactant molecules that will be beneficial for the catalytic performance.

3.3. Chemical composition in the bulk of CuO

Chemical composition in the bulk of CuO NPs was investigated using EDS. Figure 5 displays the EDS spectrum characteristic of CuO NPs with nanostructures. The obtained peaks correspond to the atomic percentages of oxygen (O: 49.24%) and copper (Cu: 50.76%). The presence of Cu and O, free of all other metals and contaminants, has been therefore confirmed by this analysis. The O/Cu atomic ratio (r = 0.97) is ~1 for the sample studied. The ratio correspond well to the copper oxide formula and correlate well with the data reported in the literature [34].

3.4. Surface chemical composition and ionic states of CuO

The Cu 2p and O 1s core shell and results of CuO NPs catalyst are shown on Figure 6 and summarized in Table 1. Figure 6 (a) present the XPS core shell of Cu 2p exhibiting a doublet at higher (Cu $2p_{1/2}$) and lower (Cu $2p_{3/2}$) binding energy (BE) located at 931.7 and 951.6 eV respectively with a spin–orbit coupling energy gap of ~20 eV, in excellent agreement with previous reported work [35, 36]. Beside the Cu 2p peaks, two other satellite peaks located respectively at ~942.19 and ~962.45 eV were observed [37, 38]. Since the discrimination of different Cu oxidation states (Cu^0 Cu^+ and Cu^{2+}) by XPS cannot be easily performed, Auger spectrum was recorded and shown on Figure 6b. As displayed in Fig. 6b, a comparison with the characteristic feature of Cu LMM BE located at ~569.5 eV indicates Cu^0 and Cu^+ do not seem to be present in the as-prepared CuO NPs in agreement with recent literature [39, 40].

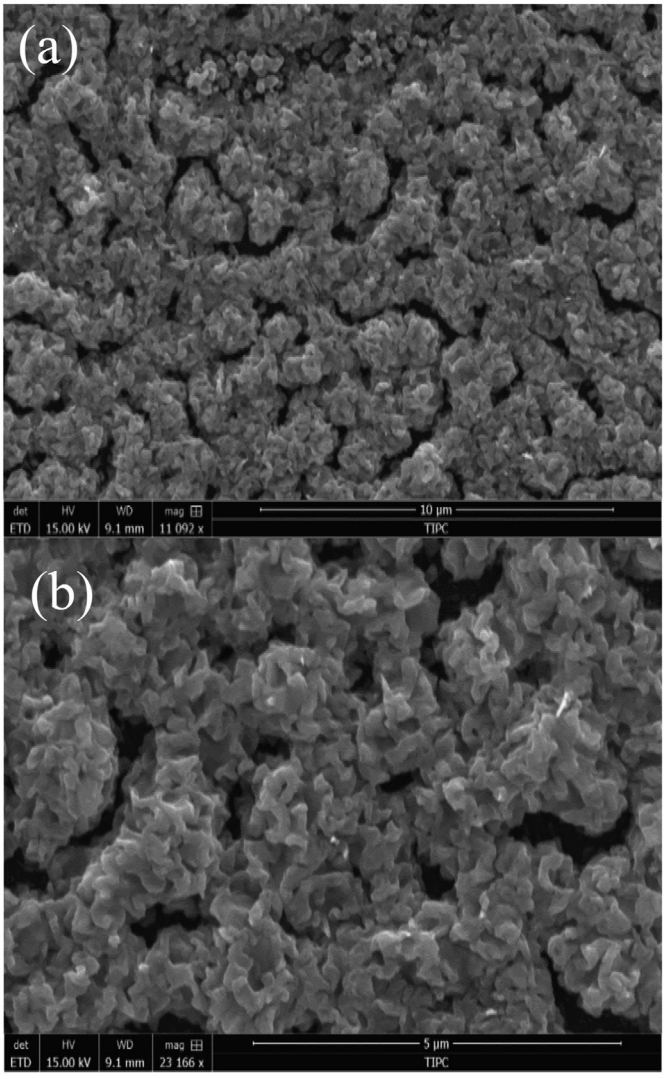

Figure 4. SEM image at two magnifications: a)10 µm and b) 5 µm of CuO NPs.

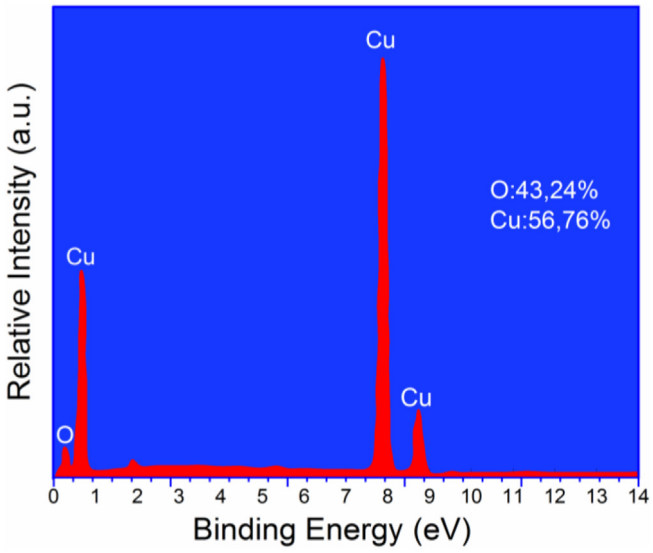

Figure 5. EDS map of CuO NPs with atomic percentage.

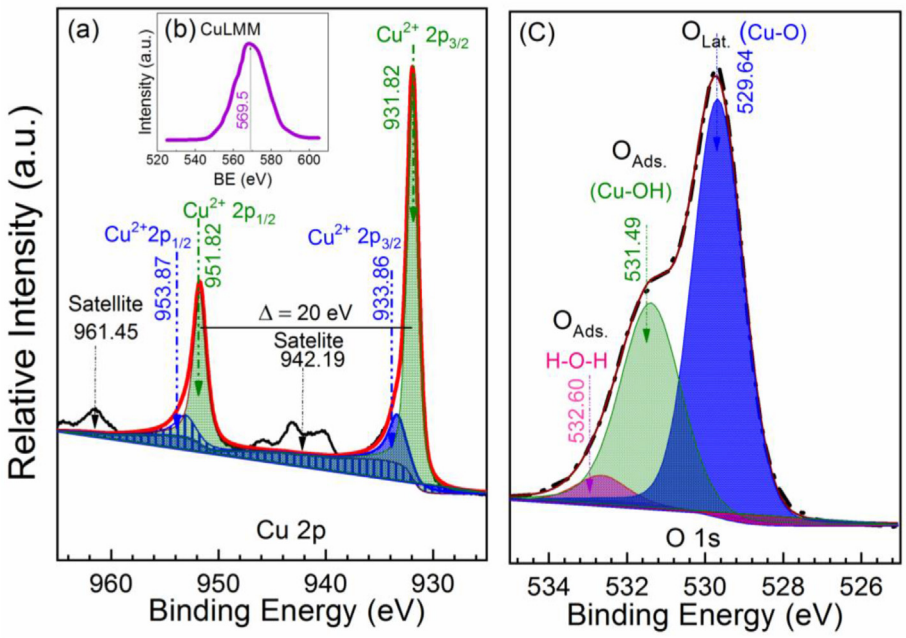

Figure 6. (a) XPS spectrum of the Cu 2p and (b) CuLMM spectrum and (c) O 1s core shell at the surface of CuO NPs prepared by precipitation.

Table 1. Physico-chemical properties, Cu 2p and O 1s peak area ratio of the as-synthesized CuO NPs.

	PS (nm)	S_{BET} (m^2/g)	Ea (kJ/mol)	H_2-TPR (°C)	XPS				
					Cu^{2+}	O_{Lat} (O_2^-)	O_{Ads} (–OH)	O_{Ads} (CO_3^{2-})	O_{Ads}/O_{Lat}
					At% BE (eV)	At%; BE (eV)	At% BE (eV)	At% BE (eV)	0.56
CuO	14	87.0	55.5	254	100 931.80	64.08 529.5	31.42 531.8	4.5 532.9	

Therefore, one can conclude that, the oxidation state of copper in the sample is mainly Cu^{2+}. The energy difference between the Cu $2p_{1/2}$ (~931.7 eV) and the corresponding satellite signal (~943.24 eV) is 11.5 eV confirmed the presence of Cu^{2+} [41]. The observed results are in agreement with XPS spectra of CuO previously published in the literature [42, 43].

The O 1s spectrum shown in Figure 6 b present two prominent peaks that have been deconvoluted into three peaks with BEs within the range of ~529.61–~531.37 eV. The lowest BE of ~529.60 eV represent the lattice oxygen ($O_{Lat.}$) detected in the form of electrophilic oxygen (O^{2-}, O_2^{2-}). The other two signals which are expanded until ~531.50 eV, were attributed to the adsorbed oxygen ($O_{Ads.}$) at the surface of CuO and present in the form of hydroxylic group (OH) in the Cu–OH bond. Finally, the band located at ~532.60 eV can be due to water moisture in the air [44]. The observed BE values of all species in this investigation are in agreement with those reported in the literature [45, 46]. Generally, it is admitted that the catalytic oxidation might be influenced by the $O_{Lat.}$ and/or $O_{Ads.}$ at the surface TMOs. Therefore, $O_{Lat.}$ and $O_{Ads.}$ detected on the CuO catalyst are expected to play a key roles in the catalytic process [47].

3.5. Optical properties

The optical band gap energy (Eg) is among of the properties that could be used to reflect the performance oxide materials. For instance, metal oxides catalysts with lower optical Eg, have been proven to demonstrate better catalytic activity [9, 48]. CuO is a p-type semiconductor with an Eg ranging from 1.3 to 2.8 eV [40, 49, 50]. The UV-Visible spectrum (Figure 7a) and the Tauc's plot (Figure 7b) are merged and presented on Figure 7. Figure 7 b depicts the plots of $(\alpha Eg)^2$ vs Eg, which is based on the direct transition. The E_g of CuO is 2.65 ± 0.05 eV obtained by extrapolating to the abscissa the straight part of the

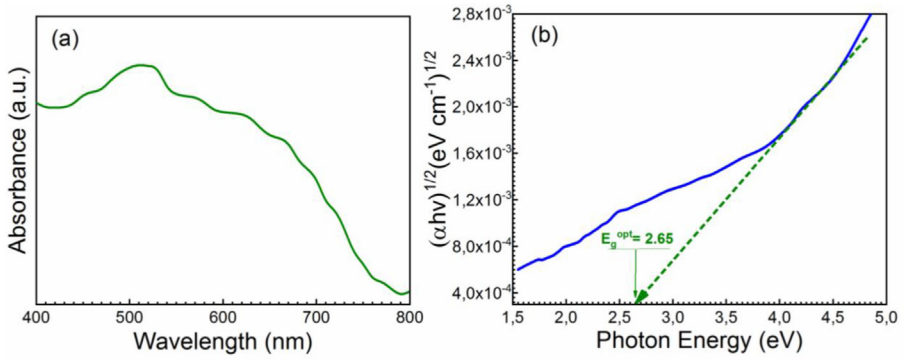

Figure 7. (a) Optical absorption spectrum and (b) Tauc plot of CuO NPs.

Tauc's plot. A strong correlation of Eg and the catalytic performance of a single (V_2O_3) and binary (FeCoO) oxide has been earlier reported [48, 51] and the authors have concluded that, TMOs with lower optical Eg exhibits good electron mobility thus better $O_{Lat.}$ mobility and reducibility which are crucial for the improvement of the catalyst performance.

3.6. TPR-H_2 analysis

The reducibility of CuO catalyst was studied by an in-situ monitoring approach (H_2-TPR). Numerous investigation have revealed for pure CuO a significant signal centered at ~ 300 °C [52, 53]. Figure 8 displays the H_2-TPR profiles of CuO, generated by integrating the absorption bands characteristic of the Cu–O stretching vibration mode. In the present work, the total reduction of CuO was achieved at 254 °C as illustrated on Figure 8 and that can be assigned to the stepwise reduction of CuO (Cu (II) to Cu(I)) generally possible at low temperature. A comparison of the curve shape and the reduction temperature with that of the above-mentioned literature suggests that, the low value obtained here might be due to the reduction of isolated bulk CuO. In addition, XRD and Raman analysis exhibits small CuO particles sizes with strong interaction between each other. Thus, the shift of CuO single and symmetrical band toward a low temperature (254 °C) is a consequence of to the presence of small grains size in the catalyst surface.

3.7. Catalytic activity

To investigate the performance of CuO, CO and C_7H_8 were selected as target pollutants and their total conversion was investigated within the temperature ranging from 100 to 400 °C and depicted on Figure 9. Earlier investigations on the CO and C_7H_8 total oxidation over bulk CuO does not display activity in below 200 °C [54, 55, 56, 57, 58, 59, 60, 61]. However, in the present work, the conversion of CO (Figure 9 a) and C_7H_8 (Figure 9 b) over CuO NPs begin at ~165 and ~170 °C and the total conversion was achieved at ~265 °C (CO) and ~300 °C (C_7H_8) respectively. The light-off curves of CO and C_7H_8 conversion over the as-synthetized CuO NPs and other catalysts such as CuO [54], Fe_2O_3 [55], Co_3O_4 [56], $CoFe_2O_4$ [57], pt/Al_2O_3 [58], CuO [59], CuCeO [59], PtPd/AlCe [60], LaFeO [61], LaMnO [61] reported in the literature are shown in Figure 9. In general, it is observed that, the total conversion of both pollutants (CO and C_7H_8) produces CO_2 and H_2O. Compared with the above listed catalysts from earlier reported works, CuO NPs catalyst in this work is the most performant.

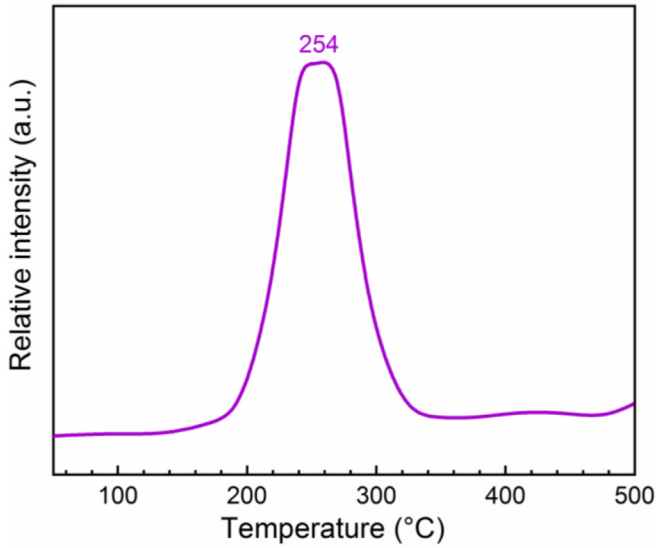

Figure 8. H_2-TPR profile of CuO NPs catalyst.

Starting at ~150 °C, CO oxidation begin at ~175 °C and the total oxidation is achieved at ~ 252 °C, relatively the lowest reaction temperature than those reported in the literature (see Figure 9a). Table 2 display the comparison of the temperature at 90 (T_{90}) and 50 % (T_{50}) conversion of CO over CuO in this study and over other TMOs including: CuO [54]; Fe_2O_3 [55]; Co_3O_4 [56]; $CoFe_2O_4$ [57] and Pt/Al_2O_3 [58], reported in the literature. The performance of the as-prepared CuO towards total CO oxidation as function of catalytic test condition was achieved at substantially lower temperatures than those of catalysts reported in the literature [54, 55, 56, 57, 58].

As far as the C_7H_8 destruction displayed on Figure 10 b and the corresponding comparison in Table 3 is concerned, it is obvious that, CuO catalyst exhibits the best catalytic efficiency, for which T_{90} and T_{50} were achieved at ~ 271 and ~237 °C respectively, temperatures much lower than of CuO, CuCeO, and Pt/Pd/AlCe catalysts earlier reported [59, 60, 61]. Total oxidation of C_7H_8 on CuO in the present work was achieved at lower temperatures when compared to metal oxide catalysts described in the literature.

In order to attest on the reusability as well as the results replicability, CuO sample was exposed several consecutives runs as displayed on Figure 10. With this test, we wanted also to test CuO susceptibility to experience thermal deactivation which will usually accounts for their limited application in industrial field. The obtained results displayed on Figure 10 (a and b) shows that, CuO exhibits excellent C_7H_8 conversion in three consecutive repeated runs and the results confirmed that CuO is reusable and reproducible. Therefore, CuO is considered as an excellent single oxide material for CO and C_7H_8 deep oxidation with a promising catalytic application.

Several factors that usually influence the catalytic performance of TMOs includes the surface morphology, BET specific surface area, oxygens vacancies, active species distribution and low-temperature reducibility. To understand the performance of CuO towards the total conversion of CO and C_7H_8, it is useful to consider the influence of H_2-TPR experiments performed on CuO. In fact, a shift of reduction temperature towards low value was observed and was attributed to occurrence of CuO small particles sizes that have enhanced the reducibility of copper species at low temperature. Accordingly, it is therefore possible to connect the shift of the reduction temperature of CuO catalysts with a high BET surface area values (~87 m^2/g). This might favoured higher lattice oxygen mobility probably as a consequence of higher structural defects induced. Based on the previous references [62, 63, 64], Mars-Van-Krevelen (MvK) mechanism is established as plausible mechanism for CO and VOCs and exhausts gas over TMOs implying $O_{Latt.}$ ions as the most active oxygen species. Generally, CO oxidation process may consist of three main steps: Firstly, CO molecule can react with $O_{Lat.}$ presents at the surface of CuO to form CO_2, enabling formation of surface oxygen vacancy (O_v); In the second step gas-phase O_2 is adsorbed at the O_v site; and finally, a second CO molecule reacts with the adsorbed O_2, yielding CO_2 and follows by catalyst surface regeneration. In other respect, CO oxidation can be achieved at low reaction temperature (165–200 °C) through degradation of surface carbonyl group (CO_3^{2-}) adsorbed at the catalysts surface [65, 66]. However, in the present work CO is obtained at temperature (<200 °C) for which a higher lattice oxygen mobility is possible. XPS results (Figure 6a) confirmed the presence of O_{Lat} (O^{2-}, O_2^{2-}) $O_{Ads.}$ (CO_3^{2-} and ^-OH) as well as moisture over CuO NPs. From the light-off curves (Figure 9a), it is thus suggested that, CO oxidation over CuO NPs might follows MvK mechanism [67]. As far as Toluene is concerned, it has been established that, complete oxidation to CO_2 and H_2O is achieved through MvK process [59, 60, 61]. However, Qin et al. [68], have recently report the coexistence of Langmuir–Hinshelwood (LH) and MvK mechanism in the toluene total oxidation over manganese-based oxides catalysts. In fact, surface $O_{Lat.}$ can react with the C_7H_8 at the temperature <200 °C, via MvK mechanism however the adsorbed oxygen species with good mobility is also found to start up and participate in the reaction at lower temperatures, which follows the LH reaction mechanism [68]. Therefore, in order to better

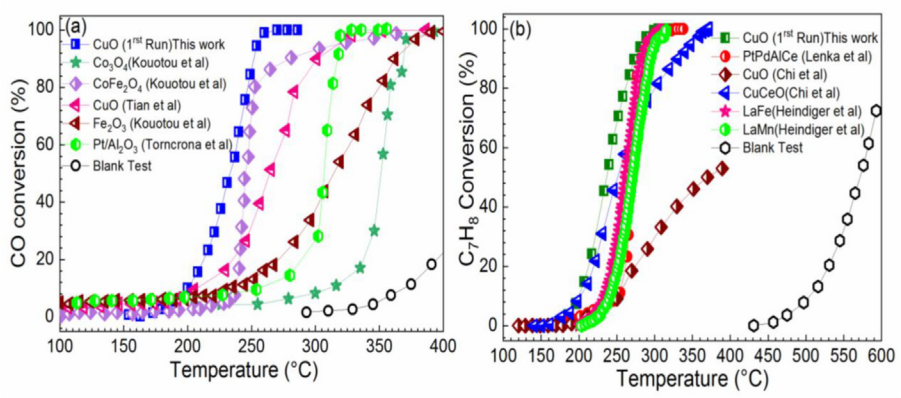

Figure 9. Conversion curves of (a) CO and (b) C_7H_8 as function of reactions temperatures over CuO NPs and other single, binary and noble metal catalysts form earlier reported investigation the literature [54, 55, 56, 57, 58, 59, 60, 61] for comparison.

Table 2. Comparison of CO oxidation over CuO in this work with several catalysts reported in the literature.

Catalysts	Weight (mg)	Gas composition	GHSV‡ (mLg^{-1} h^{-1})	Temperature		Ref.
				T_{50} (°C)	T_{90} (°C)	
CuO	60	5% CO/20% O_2 in Ar	20,000	233	252	TW§
CuO	12	1% CO/10% O2 in Ar	75,000	264	300	[54]
Fe_2O_3	20	1% CO/10% O2 in Ar	45,000	315	362	[55]
Co_3O_4	12	1% CO/10% O2 in Ar	75,000	350	368	[56]
$CoFe_2O_4$	20	1% CO/10% O2 in Ar	45,000	245	280	[57]
Pt/Al_2O_3	2/200	1% CO/1.38% O_2 in N_2	90,000	306	318	[58]

‡ GHSV: stands for gas hourly space velocity, and.
§ TW denotes the outcomes of this study.

account on the process involved in the CO and Toluene oxidation over CuO NPs the in-situ DRIFT was used.

3.8. Study of the reaction pathway for CO and C_7H_8

CO and C_7H_8 total conversion tests were performed and the reaction mechanism has been explored. The in-situ DRIFTS spectra of CO oxidation over CuO NPs at different temperatures were recorded and display in Figure 11. The typical bands of CO were located at the wavelength in the range of 2110–2170 cm^{-1}, while those of various carbonate vibrations bands appeared at 1300-1700 cm^{-1}. Upon reaction temperatures increase in the range of 100–500 °C, the typical bands of CO at 2117–2178 cm^{-1} remained unaltered, attesting that the CuO NPs catalyst exhibits a stable ability to adsorb CO. Upon a continuous increase of the reaction temperatures, the absorbance CO_3^{2-} vibrations located at 1300-1700 cm^{-1} was decreasing while those of CO (2110-2170 cm^{-1}) started increasing as an indication that, the total oxidation of CO to CO_3^{2-} was accelerated [69]. At the reaction temperature of ~250 °C, the absorption band at 2110 –2170 cm^{-1} and that at 1735 cm^{-1} has of almost disappeared, indicating that CO_3^{2-} species were more decomposed at ~250 °C and finally transformed to CO_2. Of the foregoing, conversion process of CO to CO_2 onto CuO NPs might be as follows: CO was adsorbed on the CuO NPs surface (1rst step), follows by their oxidation in the presence of active oxygen species to CO_3^{2-}, (2nd step) and finally, CO_3^{2-} were transformed to CO_2 (3rd step).

Based on the discussion above, CO and C_7H_8 total conversion was proposed to follow a MvK mechanism as displayed in Figure 12. CO (A) and C_7H_8 (B) pathway involve three main steps: (I) O_2 molecules adsorption and activation; (II) CO/C_7H_8 molecules adsorption on the surface-active sites Cu^{2+} of CuO NPs; conversion of CO/C_7H_8 molecules into the reaction intermediates as the temperature increase in agreement with the literature [70, 71].

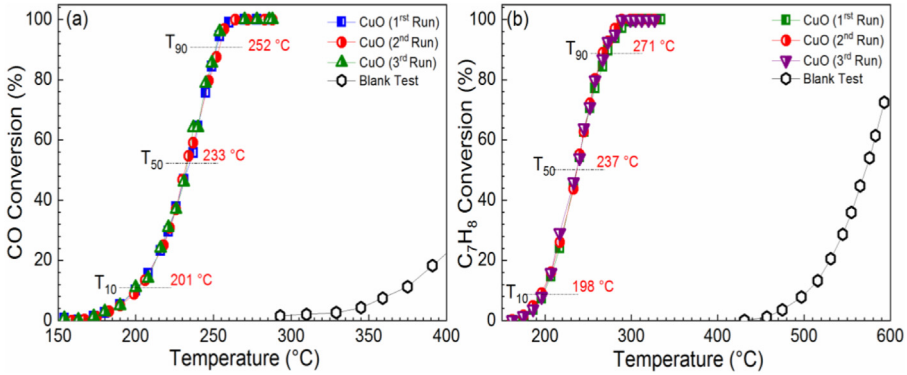

Figure 10. Total conversion of (a) CO and (b) C_7H_8 as a function of the reaction temperature upon three consecutive cycles.

Table 3. Comparison of C_7H_8 oxidation over CuO in this work with several catalysts reported in the literature.

Catalysts	Weight (mg)	Gas composition	GHSV[‡] (mLg^{-1} h^{-1})	Temperature		Ref.
				T_{50} (°C)	T_{90} (°C)	
CuO	60	5% C_7H_8/20% O_2 in Ar	20,000	237	271	TW[§]
CuO	300	1% C_7H_8/21% O_2 in N_2	36,000	269	-	[59]
CuCeO	300	1% C_7H_8/21% O_2 in N_2	36,000	249	322	[59]
Pt/Pd/AlCe	225	2% C_7H_8/21% O_2 in N_2	71,000	270	285	[60]
LaFeO	200	1% C_7H_8/20% O_2 in N_2	100,000	261	283	[61]
LaMnO	200	1% C_7H_8/20% O_2 in N_2	100,000	271	295	[61]

3.9. Catalytic stability and durability

The catalyst stability or durability in the catalytic oxidation process is well established as an important characteristic for the catalysts application at industrial scale [70]. To investigate on the catalytic stability of the CuO NPs, the long-term time-on-stream (TOS) of oxidation of CO and C_7H_8 was performed for 30 h, and the results are displayed in Figure 13. The experimental conditions for the durability test were as following: (a) 60 mL.$min^{-1}$of CO in the feed gas, GHSV of 72 000 $mLg^{-1}h^{-1}$, reaction temperature of 260 °C; (b) 75 $mLg^{-1}h^{-1}$ of C_7H_8 in the feed gas, at constant temperature of 300 °C, reaction time of 30 h, GHSV of 20 000 $mLg^{-1}h^{-1}$, and the conversion of CO and toluene over CuO was almost 100% from the activity test at 260 and 300 °C respectively under time-on-stream of 30h. During the long-term running, CuO NPs showed remarkably perfect CO and toluene conversion as well as excellent reaction stability ranging between 95% and 98% for 30 h. Despite some minor variations observed during the process, the conversion was kept at a high level. Therefore, in addition to the high performance, CuO NPs exhibited excellent stability or durability in the long-term TOS test, which was of crucial significance for the industrial application.

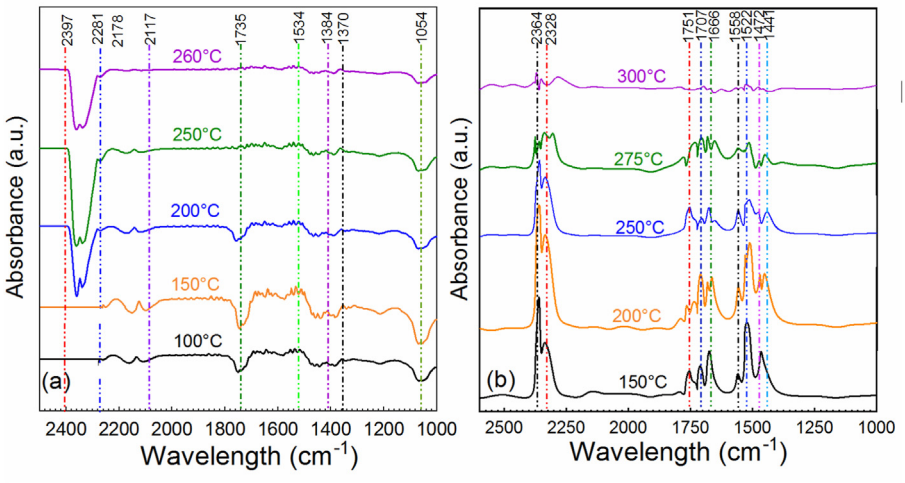

Figure 11. In situ DRIFTS spectra of CuO NPs in: (a) 5%CO20%O_2/in Ar and (b) 500ppm/CO20%O_2/in Ar at different temperatures.

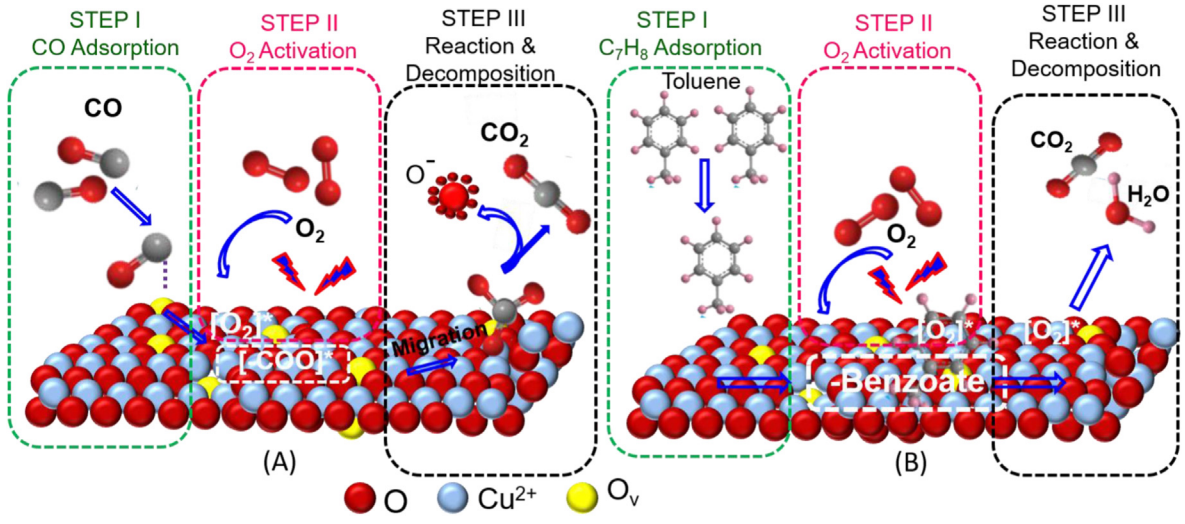

Figure 12. The reaction mechanism of: A) CO and B) C_7H_8 oxidation over CuO NPs catalyst. Adapted with permission from Zhang et al. [71], and Mo et al., [72].

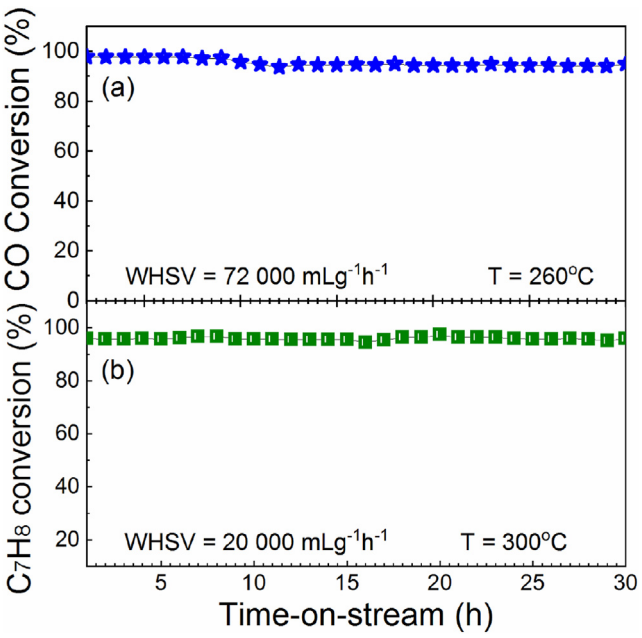

Figure 13. Stability and durability tests for CO and C_7H_8 oxidation in single component with time-on-stream over CuO: (a) 60 mL.min^{-1}of CO in the feed gas, reaction temperature of 260 °C, reaction time of 30 h, GHSV of 72 000 mLg^{-1}h^{-1}; (b) 75 mLg^{-1}h^{-1}; of C_7H_8 in the feed gas, reaction temperature of 300 °C, reaction time of 30 h, GHSV of 20 000 mLg^{-1}h^{-1}.

4. Conclusion

This study was focused on CuO preparation for the catalytic application. The structure, morphology, composition, and ionic states of the as-prepared catalyst, as well as the optical energy band gap characteristics, were all studied. In addition, H_2-TPR was carried out to determine the reduction property of the as-prepared single oxide. XRD, FTIR, and Raman analysis confirmed the obtained oxide as CuO, with a monoclinic structure. The analysis of the surface microstructure by SEM shows CuO was homogeneous and well covered with fine interconnected particles. The bulk (EDS) and surface chemical composition (XPS) attest on the occurrence of Copper and Oxygen as main elements with Cu^{2+}, O^{2-} and OH^- as their corresponding ionic oxidation states. Finally, the obtained catalyst was tested with success as catalyst toward total conversion of CO and C_7H_8 and surprisingly, CuO exhibits better performance than single and binary oxides and comparable performance compared with supported noble metals catalyst reported in the literature. The results indicate that CuO is an effective and eco-friendly oxide catalyst for the degradation of VOCs and exhausts gas. The observed excellent performance of CuO NPs is suggested to be due to porous-like structure with large specific surface area that offer more exposed unsaturated coordination sites beneficial for the CO and C_7H_8 total conversion at low temperature via MvK mechanism. More importantly, it was observed that in addition to the excellent performance, CuO NPs catalysts exhibited good stability in the prolonged isothermal test. In consequence, CuO NPs display great potential for the catalytic oxidation of VOCs and exhaust gas at the industrial scale.

Declarations

Author contribution statement

Hippolyte Todou Assaouka: Performed the experiments, Analyzed and interpreted the data; Wrote the paper.

Daniel Manhouli Daawe, Roussin Lontio Fomekong: Conceived and designed the experiments; Performed the experiments.

Issah Njiawouo Nsangou: Performed the experiments; Analyzed and interpreted the data.

Patrick Mountapmbeme Kouotou: Conceived and designed the experiments; Analyzed and interpreted the data; Contributed reagents, materials, analysis tools or data.

Funding statement

This research did not receive any specific grant from funding agencies in the public, commercial, or not-for-profit sectors.

Data availability statement

Data will be made available on request.

Declaration of interests statement

The authors declare no conflict of interest.

Additional information

No additional information is available for this paper.

References

[1] X. Yao, L. Zhang, L. Li, L. Liu, Y. Cao, X. Dong, F. Gao, Y. Deng, C. Tang, Z. Chen, Investigation of the structure, acidity, and catalytic performance of CuO/$Ti_{0.95}Ce_{0.05}O_2$ catalyst for the selective catalytic reduction of NO by NH_3 at low temperature, Appl. Catal. B Environ. 150 (2014) 315–329.

[2] A.A. Gokhale, J.A. Dumesic, M. Mavrikakis, On the mechanism of low-temperature water gas shift reaction on copper, J. Am. Chem. Soc. 130 (2008) 1402–1414.

[3] L. Wang, L. Yang, Y. Zhang, W. Ding, S. Chen, W. Fang, Y. Yang, Promoting effect of an aluminum emulsion on catalytic performance of Cu-based catalysts for methanol synthesis from syngas, Fuel Process. Technol. 91 (2010) 723–728.

[4] J.J. Spivey, Complete catalytic oxidation of volatile organics, Ind. Eng. Chem. Res. 26 (1987) 2165–2180.

[5] M.F. Zwinkels, S.G. Järås, P.G. Menon, T.A. Griffin, Catalytic materials for high-temperature combustion, Catal. Rev. Sci. Eng. 35 (1993) 319–358.

[6] E.M. Cordi, J.L. Falconer, Oxidation of volatile organic compounds on Al_2O_3, Pd/Al_2O_3, and PdO/Al_2O_3 Catalysts, J. Catal. 162 (1996) 104–117.

[7] D.A. Pena, B.S. Uphade, P.G. Smirniotis, TiO_2-supported metal oxide catalysts for low-temperature selective catalytic reduction of NO with NH_3: I. Evaluation and characterization of first row transition metals, J. Catal. 221 (2004) 421–431.

[8] Z. Hu, Y. Peng, Z. Kang, Y. Qian, D. Zhao, A modulated hydrothermal (MHT) approach for the facile synthesis of UiO-66-type MOFs, Inorg. Chem. 54 (2015) 4862–4868.

[9] Z.Y. Tian, N. Bahlawane, F. Qi, K. Kohse-Höinghaus, Catalytic oxidation of hydrocarbons over Co_3O_4 catalyst prepared by CVD, Catal. Commun. 11 (2009) 118–122.

[10] X. Xie, Y. Li, Z.-Q. Liu, M. Haruta, W. Shen, Low-temperature oxidation of CO catalysed by Co_3O_4 nanorods, Nature 458 (2009) 746–749.

[11] Z.Y. Tian, P.H.T. Ngamou, V. Vannier, K. Kohse-Höinghaus, N. Bahlawane, Catalytic oxidation of VOCs over mixed Co–Mn oxides, Appl. Catal. B Environ. 117 (2012) 125–134.

[12] X. Mou, X. Wei, Y. Li, W. Shen, Tuning crystal-phase and shape of Fe_2O_3 nanoparticles for catalytic applications, CrystEngComm 14 (2012) 5107–5120.

[13] F. Pu, Y. Bai, J. Lv, X. Zhao, G. Wu, C. Kong, B. Lei, X. Zhang, H. Jin, Z. Yang, Yolk–shell Cu_2O@ CuO-decorated RGO for high-performance lithium-ion battery anode, Energy Environ. Mater. 5 (2022) 253–260.

[14] M.B. Gawande, A. Goswami, F.-X. Felpin, T. Asefa, X. Huang, R. Silva, X. Zou, R. Zboril, R.S. Varma, Cu and Cu-based nanoparticles: synthesis and applications in catalysis, Chem. Rev. 116 (2016) 3722–3811.

[15] S. Royer, D. Duprez, Catalytic oxidation of carbon monoxide over transition metal oxides, ChemCatChem 3 (2011) 24–65.

[16] S.B. Wang, C.H. Hsiao, S.J. Chang, K.T. Lam, K.H. Wen, S.C. Hung, S.J. Young, B.R. Huang, A CuO nanowire infrared photodetector, Sensor Actuator Phys. 171 (2011) 207–211.

[17] T. Umegaki, Y. Kojima, K. Omata, Effect of oxide coating on performance of copper-zinc oxide-based catalyst for methanol synthesis via hydrogenation of carbon dioxide, Materials 8 (2015) 7738–7744.

[18] A. Arango-Díaz, E. Moretti, A. Talon, L. Storaro, M. Lenarda, P. Núnez, J. Marrero-Jerez, J. Jiménez-Jiménez, A. Jiménez-López, E. Rodríguez-Castellón, Preferential CO oxidation (CO-PROX) catalyzed by CuO supported on nanocrystalline CeO_2 prepared by a freeze-drying method, Appl. Catal. Gen. 477 (2014) 54–63.

[19] C. Anil, G. Madras, Kinetics of CO oxidation over Cu doped Mn_3O_4, J. Mol. Catal. Chem. 424 (2016) 106–114.

[20] Y. Bu, J.H. Niemantsverdriet, H.O. Fredriksson, Cu model catalyst dynamics and CO oxidation kinetics studied by simultaneous in situ UV–Vis and mass spectroscopy, ACS Catal. 6 (2016) 2867–2876.

[21] M. Abecassis-Wolfovich, H. Rotter, M.V. Landau, E. Korin, A.I. Erenburg, D. Mogilyansky, E. Gartstein, Texture and nanostructure of chromia aerogels prepared by urea-assisted homogeneous precipitation and low-temperature supercritical drying, J. Non-Cryst. Solids 318 (2003) 95–111.

[22] H. Tajizadegan, O. Torabi, A. Heidary, M.H. Golabgir, A. Jamshidi, Study of methyl orange adsorption properties on $ZnO–Al_2O_3$ nanocomposite adsorbent particles, Desalination Water Treat. 57 (2016) 12324–12334.

[23] W. Deng, M. Flytzani-Stephanopoulos, On the deactivation of nanostructured gold-ceria and platinum-ceria catalysts for the water-gas shift reaction in practical fuel cell applications, Angew. Chem. Int. Ed. 45 (2006) 2285–2289.

[24] G. Qiu, S. Dharmarathna, Y. Zhang, N. Opembe, H. Huang, S.L. Suib, Facile microwave-assisted hydrothermal synthesis of CuO nanomaterials and their catalytic and electrochemical properties, J. Phys. Chem. C 116 (2012) 468–477.

[25] N.V. Suramwar, S.R. Thakare, N.T. Khaty, Synthesis and catalytic properties of nano CuO prepared by soft chemical method, Int. J. Nano Dimens. (IJND) 3 (2012) 75–80.

[26] J. Li, P. Zhu, S. Zuo, Q. Huang, R. Zhou, Influence of Mn doping on the performance of CuO-CeO_2 catalysts for selective oxidation of CO in hydrogen-rich streams, Appl. Catal. A General. 381 (2010) 261–266.

[27] S.-H. Zeng, C.-W. Chen, L. Hong, J.-H. Liu, X.-X. Deng, In vitro induction, regeneration and analysis of auto-tetraploids derived from protoplasts and callus treated with colchicine in Citrus, Plant Cell Tissue Organ Cult. 87 (2006) 85–93.

[28] G. Kliche, Z.V. Popovic, Far-infrared spectroscopic investigations on CuO, Phys. Rev. B 42 (1990), 10060.

[29] T. Yu, X. Zhao, Z.X. Shen, Y.H. Wu, W.H. Su, Investigation of individual CuO nanorods by polarized micro-Raman scattering, J. Cryst. Growth 268 (2004) 590–595.

[30] M.H. Chou, S.B. Liu, C.Y. Huang, S.Y. Wu, C.-L. Cheng, Confocal Raman spectroscopic mapping studies on a single CuO nanowire, Appl. Surf. Sci. 254 (2008) 7539–7543.

[31] Y.S. Gong, C. Lee, C.K. Yang, Atomic force microscopy and Raman spectroscopy studies on the oxidation of Cu thin films, J. Appl. Phys. 77 (1995) 5422–5425.

[32] A. Chapelle, M.H. Yaacob, I. Pasquet, L. Presmanes, A. Barnabé, P. Tailhades, J. Du Plessis, K. Kalantar-Zadeh, Structural and gas-sensing properties of CuO–$Cu_xFe_{3-x}O_4$ nanostructured thin films, Sensor. Actuator. B Chem. 153 (2011) 117–124.

[33] A. Gurbani, J.L. Ayastuy, M.P. González-Marcos, M.A. Gutiérrez-Ortiz, CuO–CeO_2 catalysts synthesized by various methods: comparative study of redox properties, Int. J. Hydrogen Energy 35 (2010) 11582–11590.

[34] L.-P. Zhu, N.-C. Bing, L.-L. Wang, H.-Y. Jin, G.-H. Liao, L.-J. Wang, Self-assembled 3D porous flowerlike α-Fe_2O_3 hierarchical nanostructures: synthesis, growth mechanism, and their application in photocatalysis, Dalton Trans. 41 (2012) 2959–2965.

[35] C.V. Schenck, J.G. Dillard, J.W. Murray, Surface analysis and the adsorption of Co (II) on goethite, J. Colloid Interface Sci. 95 (1983) 398–409.

[36] M. Oku, Y. Sato, In-situ X-ray photoelectron spectroscopic study of the reversible phase transition between CoO and Co_3O_4 in oxygen of 10^{-3} Pa, Appl. Surf. Sci. 55 (1992) 37–41.

[37] J. Papavasiliou, G. Avgouropoulos, T. Ioannides, Combined steam reforming of methanol over Cu–Mn spinel oxide catalysts, J. Catal. 251 (2007) 7–20.

[38] L. Dong, B. Zhang, C. Tang, B. Li, L. Zhou, F. Gong, B. Sun, F. Gao, L. Dong, Y. Chen, Influence of CeO_2 modification on the properties of Fe_2O_3–$Ti_{0.5}Sn_{0.5}O_2$ catalyst for NO reduction by CO, Catal. Sci. Technol. 4 (2014) 482–493.

[39] Z. Guo, M.L. Seol, M.S. Kim, J.H. Ahn, Y.K. Choi, J.H. Liu, X.J. Huang, Hollow CuO nanospheres uniformly anchored on porous Si nanowires: preparation and their potential use as electrochemical sensors, Nanoscale 4 (2012) 7525–7531.

[40] C. Song, Z. Zhao, H. Li, Wang, Y. Yang, CeO_2 decorated CuO hierarchical composites as inverse catalyst for enhanced CO oxidation, RSC Adv. 6 (2016) 102931–102937.

[41] Z. Guo, M.-L. Seol, M.-S. Kim, J.-H. Ahn, Y.-K. Choi, J.-H. Liu, X.-J. Huang, Hollow CuO nanospheres uniformly anchored on porous Si nanowires: preparation and their potential use as electrochemical sensors, Nanoscale 4 (2012) 7525–7531.

[42] A.F. Zedan, A.T. Mohamed, M.S. El-Shall, S.Y. AlQaradawi, A.S. AlJaber, Tailoring the reducibility and catalytic activity of CuO nanoparticles for low temperature CO oxidation, RSC Adv. 8 (2018) 19499–19511.

[43] C. Song, D. Zhang, J. Zhang, L. Zheng, C. Zhao, J. Ma, N. An, M. Han, Expression analysis of key auxin synthesis, transport, and metabolism genes in different young dwarfing apple trees, Acta Physiol. Plant. 38 (2016) 43.

[44] C.-S. Liu, J. Li, H. Pang, Metal-organic framework-based materials as an emerging platform for advanced electrochemical sensing, Coord. Chem. Rev. 410 (2020), 213222.

[45] G. Bhargava, I. Gouzman, C.M. Chun, T.A. Ramanarayanan, S.L. Bernasek, Characterization of the "native" surface thin film on pure polycrystalline iron: a high resolution XPS and TEM study, Appl. Surf. Sci. 253 (2007) 4322–4329.

[46] G.K. Pradhan, K.M. Parida, Fabrication, growth mechanism, and characterization of α-Fe_2O_3 nanorods, ACS Appl. Mater. Interfaces 3 (2011) 317–323.

[47] C.-F. Cheng, M.-L. Chang, C.-S. Li, Configural paths to successful product innovation, J. Bus. Res. 66 (2013) 2561–2573.

[48] B.Y. Jibril, Catalytic performances and correlations with metal oxide band gaps of metal-tungsten mixed oxide catalysts in propane oxydehydrogenation, React. Kinet. Catal. Lett. 86 (2005) 171–177.

[49] A. Chen, H. Long, X. Li, Y. Li, G. Yang, P. Lu, Controlled growth and characteristics of single-phase Cu_2O and CuO films by pulsed laser deposition, Vacuum 83 (2009) 927–930.

[50] G. Papadimitropoulos, N. Vourdas, V.E. Vamvakas, D. Davazoglou, Optical and structural properties of copper oxide thin films grown by oxidation of metal layers, Thin Solid Films 515 (2006) 2428–2432.

[51] P.M. Kouotou, H. Vieker, Z.Y. Tian, P.T. Ngamou, A. El Kasmi, A. Beyer, A. Gölzhäuser, K. Kohse-Höinghaus, Structure–activity relation of spinel-type Co–Fe oxides for low-temperature CO oxidation, Catal. Sci. Technol. 4 (2014) 3359–3367.

[52] F. Yang, J. Wei, W. Liu, J. Guo, Y. Yang, Copper doped ceria nanospheres: surface defects promoted catalytic activity and a versatile approach, J. Mater. Chem. 2 (2014) 5662–5667.

[53] S. Zeng, W. Zhang, S. Guo, H. Su, Inverse rod-like CeO_2 supported on CuO prepared by hydrothermal method for preferential oxidation of carbon monoxide, Catal. Commun. 23 (2012) 62–66.

[54] Z.Y. Tian, H.J. Herrenbrück, P.M. Kouotou, H. Vieker, A. Beyer, A. Gölzhäuser, K. Kohse-Höinghaus, Facile synthesis of catalytically active copper oxide from pulsed-spray evaporation CVD, Surf. Coating. Technol. 230 (2013) 33–38.

[55] P.M. Kouotou, Z.Y. Tian, H. Vieker, K. Kohse-Höinghaus, Pulsed-spray evaporation CVD synthesis of hematite thin films for catalytic conversion of CO, Surf. Coating. Technol. 230 (2013) 59–65.

[56] P.M. Kouotou, Z.Y. Tian, U. Mundloch, N. Bahlawane, K. Kohse-Höinghaus, Controlled synthesis of Co_3O_4 spinel with $Co(acac)_3$ as precursor, RSC Adv. 2 (2012) 10809–10812.

[57] P.M. Kouotou, Z.Y. Tian, Cobalt-iron oxides made by CVD for low temperature catalytic application, Phys. Status Solidi 212 (2015) 1508–1513.

[58] A. Törncrona, M. Skoglundh, P. Thormählen, E. Fridell, E. Jobson, Low temperature catalytic activity of cobalt oxide and ceria promoted Pt and Pd: influence of pretreatment and gas composition, Appl. Catal. B Environ. 14 (1997) 131–145.

[59] C. He, Y. Yu, L. Yue, N. Qiao, J. Li, Q. Shen, W. Yu, J. Chen, Z. Hao, Low-temperature removal of toluene and propanal over highly active mesoporous CuCeOx catalysts synthesized via a simple self-precipitation protocol, Appl. Catal. B Environ. 147 (2014) 156–166.

[60] L. Matějová, P. Topka, K. Jirátová, O. Šolcová, Total oxidation of model volatile organic compounds over some commercial catalysts, Appl. Catal. A General. 443 (2012) 40–49.

[61] B. Heidinger, Synthèse par broyage réactif de perovskites (La, Sr, Ce) (Mn, Fe, Co) O_3 : caractérisation et propriétés catalytiques dans la réaction d'oxydation totale du toluène, PhD thesis, University of Laval, 2020. http://hdl.handle.net/20.500.11794/69021.

[62] H. Lee, J.C. Jung, H. Kim, Y.-M. Chung, T.J. Kim, S.J. Lee, S.-H. Oh, Y.S. Kim, I.K. Song, Oxidative dehydrogenation of n-butene to 1,3-butadiene over ZnMe III FeO_4 catalysts: effect of trivalent metal (Me III), Catal. Lett. 131 (2009) 344–349.

[63] M. Ziemba, C. Hess, Influence of gold on the reactivity behaviour of ceria nanorods in CO oxidation: combining operando spectroscopies and DFT calculations, Catal. Sci. Technol. 10 (2020) 3720–3730.

[64] X. Yan, T. Gan, S. Shi, J. Du, G. Xu, W. Zhang, W. Yan, Y. Zou, G. Liu, Potassium-incorporated manganese oxide enhances the activity and durability of platinum catalysts for low-temperature CO oxidation, Catal. Sci. Technol. 11 (2021) 6369–6373.

[65] P.M. Kouotou, A. El Kasmi, L.-N. Wu, M. Waqas, Z.Y. Tian, Particle size-band gap energy-catalytic properties relationship of PSE-CVD-derived Fe_3O_4 thin films, J. Taiwan Inst. Chem. Eng. 93 (2018) 427–435.

[66] L.N. Wu, Z.Y. Tian, W. Qin, DFT study on CO catalytic oxidation mechanism on the defective Cu_2O (111) surface, J. Phys. Chem. C 122 (2018) 16733–16740.

[67] W. Hertl, R.J. Farrauto, Mechanism of carbon monoxide and hydrocarbon oxidation on copper chromite, J. Catal. 29 (1973) 352–360.

[68] Y. Qin, H. Wang, C. Dong, Z. Qu, Evolution and enhancement of the oxygen cycle in the catalytic performance of total toluene oxidation over manganese-based catalysts, J. Catal. 380 (2019) 21–31.

[69] B. Feng, M. Shi, J. Liu, X. Han, Z. Lan, H. Gu, X. Wang, H. Sun, Q. Zhang, H. Li, Y. Wang, H. Li, An efficient defect engineering strategy to enhance catalytic performances of Co_3O_4 nanorods for CO oxidation, J. Hazard Mater. 394 (2020), 122540.

[70] A. Aranzabal, J. Gonzalez-Marcos, M. Romero-Saez, J. Gonzalez-Velasco, M. Guillemot, P. Magnoux, Stability of protonic zeolites in the catalytic oxidation of chlorinated VOCs (1,2-dichloroethane), Appl. Catal. B Environ. 88 (2009) 533–541.

[71] Q. Zhang, S. Mo, J. Li, Y. Sun, M. Zhang, P. Chen, M. Fu, J. Wu, L. Chen, D. Ye, *In situ* DRIFT spectroscopy insights into the reaction mechanism of CO and toluene co-oxidation over Pt-based catalysts, Catal. Sci. Technol. 9 (2019) 4538–4551.

[72] S. Mo, Q. Zhang, Y. Sun, M. Zhang, J. Li, Q. Ren, M. Fu, J. Wu, L. Chen, D. Ye, Gaseous CO and toluene co-oxidation over monolithic core–shell Co_3O_4 based hetero- structured catalysts, Mater. Chem. 7 (2019) 16197–16210.